CHEMISTRY OF MATERIALS
Article

Chem. Mater. **2011,** *23,* 21–31 21
DOI:10.1021/cm102388q

Multifunctional Magnetic Molecular $\{[Mn^{II}(urea)_2(H_2O)]_2[Nb^{IV}(CN)_8]\}_n$ System: Magnetization-Induced SHG in the Chiral Polymorph

Dawid Pinkowicz,[†] Robert Podgajny,[†] Wojciech Nitek,[†] Michał Rams,[‡] Anna Małgorzata Majcher,[‡] Tomohiro Nuida,[§] Shin-ichi Ohkoshi,*[,§] and Barbara Sieklucka*[,†]

[†]*Faculty of Chemistry, Jagiellonian University, Ingardena 3, 30-060 Kraków, Poland,* [‡]*Institute of Physics, Jagiellonian University, Reymonta 4, 30-059 Kraków, Poland, and* [§]*The University of Tokyo, 7-3-1 Hongo, Bunkyo-ku, Tokyo 113-0033, Japan*

Received August 19, 2010. Revised Manuscript Received November 19, 2010

Incorporation of urea molecules into the magnetic system Mn^{II}-$[Nb^{IV}(CN)_8]$ results in formation of two magnetic polymorphs $\{[Mn^{II}(H_2O)(urea)_2]_2[Nb^{IV}(CN)_8]\}_n$ chiral α and centric β crystallizing in space groups $P4_1$ and $P\bar{1}$, respectively. Both polymorphs exhibit extremely similar structures and are soft ferrimagnets with critical temperatures of 43 and 42 K, respectively. The presence of coordinated urea in the noncentrosymmetric α produces NLO functionality, second harmonic generation (SHG), whereas centric β is just another molecular magnet. As a result of interaction of both functionalities below magnetic ordering temperature, the magnetization-induced SHG (MSHG) is observed for polymorph α. The observed MSHG/SHG signal ratio was the largest among molecule-based noncentrosymmetric magnets. The presence of urea molecules in both polymorphs gives also rise to their interesting topotactic reactivity. Both polymorphs can be easily transformed into a new entity $\{[Mn^{II}(H_2O)]_2[Nb^{IV}(CN)_8]\cdot 2.5MeOH\}_n$ **2b** with significant shift of critical temperature T_c to 70 K. Subsequent hydration of **2b** leads to $\{[Mn^{II}(H_2O)_2]_2[Nb^{IV}(CN)_8]\cdot 4H_2O\}_n$ **3** with T_c of 47 K.

1. Introduction

Extensive research in the field of molecular magnetism, has led to the synthesis of many various molecule-based magnets including very attractive room temperature magnets[1] and single molecule magnets[2] (SMM). Recently, much attention has been devoted to attain multifunctional magnetic molecular materials[3] (4Ms) like photo-induced magnets[4] or magnetic sponges[5] with possible applications as molecular switches, chemical sensors, and for the construction of alternative data-storage devices.

Introduction of particular symmetry features that break parity-reversal symmetry into the structures of molecular magnets, where breaking of time-reversal symmetry occurs (because of the spontanous magnetization),[6] led to the discovery of new phenomena of magneto-chiral dichroism (MChD)[7] in chiral magnets and magnetization-induced

*Corresponding author. E-mail: ohkoshi@chem.s.u-tokyo.ac.jp ; barbara.sieklucka@uj.edu.pl.

(1) (a) Manriquez, J. M.; Yee, G. T.; Mclean, R. S.; Epstein, A. J.; Miller, J. S. *Science* **1991**, *252*, 1415. (b) Ferlay, S.; Mallah, T.; Ouahès, R.; Veillet, P.; Verdaguer, M. *Nature* **1995**, *378*, 701. (c) Holmes, S. M.; Girolami, G. S. *J. Am. Chem. Soc.* **1999**, *121*, 5593.
(2) (a) Gatteschi, D.; Caneschi, A.; Pardi, L.; Sessoli, R. *Science* **1994**, *265*, 1054. (b) Sessoli, R.; Gatteschi, D.; Caneschi, A.; Novak, A. M. *Nature* **1993**, *365*, 141.
(3) (a) Verdaguer, M.; Bleuzen, A.; Marvaud, V.; Vaissermann, J.; Seuleiman, M.; Desplanches, C.; Train, C.; Garde, R.; Gelly, G.; Lomenech, C.; Rosenman, I.; Veillet, P.; Cartier, C.; Villain, F. *Coord. Chem. Rev.* **1999**, *190*−*192*, 1023–1047. (b) Sieklucka, B.; Podgajny, R.; Przychodzeń, P.; Korzeniak, T. *Coord. Chem. Rev.* **2005**, *249*, 2203–2221. (c) Pardo, E.; Train, C.; Lescouëzec, R.; Journaux, Y.; Pasán, J.; Ruiz-Pérez, C.; Delgado, F. S.; Ruiz-Garcia, R.; Lloret, F.; Paulsen, C. *Chem. Commun.* **2010**, *46*, 2322–2324.
(4) (a) Ohkoshi, S.; Hashimoto, K. *J. Photochem. Photobiol. C: Photochem. Rev.* **2001**, *2*, 71–88. (b) Shimamoto, N.; Ohkoshi, S.; Sato, O.; Hashimoto, K. *Inorg. Chem.* **2002**, *41*, 678–684. (c) Bleuzen, A.; Marvaud, V.; Mathoniere, C.; Sieklucka, B.; Verdaguer, M. *Inorg. Chem.* **2009**, *48*, 3453–3466.
(5) (a) Larionova, J.; Chavan, S. A.; Yakhmi, J. V.; Gulbrandsen Frøystein, A.; Sletten, J.; Sourisseau, C.; Kahn, O. *Inorg. Chem.* **1997**, *36*, 6374–6381. (b) Larionova, J.; Clérac, R.; Sanchiz, J.; Kahn, O.; Golhen, St.; Ouahab, L. *J. Am. Chem. Soc.* **1998**, *120*, 13088–13095. (c) Kahn, O.; Larionova, J.; Yakhmi, J. V. *Chem.—Eur. J.* **1999**, *5*, 3443–3449. (e) Yanai, N.; Kaneko, W.; Yoneda, K.; Ohba, M.; Kitagawa, S. *J. Am. Chem. Soc.* **2007**, *129*, 3496–3497. (f) Kaneko, W.; Ohba, M.; Kitagawa, S. *J. Am. Chem. Soc.* **2007**, *129*, 13706–13712. (g) Yoshida, Y.; Inoue, K.; Kurmoo, M. *Inorg. Chem.* **2009**, *48*, 10726–10736.
(6) Birss, R. R. *Symmetry and Magnetism*; North Holland: Amsterdam, 1964; Vol. *3*.
(7) (a) Rikken, G. L. J. A.; Raupach, E. *Nature* **1997**, *390*, 493. (b) Train, C.; Gheorghe, R.; Krstic, V.; Chamoreau, L.-M.; Ovanesyan, N. S.; Rikken, G. L. J. A.; Gruselle, M.; Verdaguer, M. *Nat. Mater.* **2008**, *7*, 729. (c) Inoue, K.; Imai, H.; Ghalsasi, P. S.; Kikuchi, K.; Ohba, M.; Ōkawa, H.; Yakhmi, J. V. *Angew. Chem., Int. Ed.* **2001**, *40*, 4242. (d) Coronado, E.; Galán-Mascarós, J. R.; Gómez-García, C. J.; Martínez-Ferrero, E.; Almeida, M.; Waerenborgh, J. C. *Eur. J. Inorg. Chem.* **2005**, 2064. (e) Kumaiga, H.; Inoue, K. *Angew. Chem., Int. Ed.* **1999**, *38*, 1601. (f) Minguet, M.; Luneau, D.; Lhotel, E.; Villar, V.; Paulsen, C.; Amabilino, D. B.; Veciana, J. *Angew. Chem., Int. Ed.* **2002**, *41*, 586. (g) Coronado, E.; Gómez-García, C. J.; Nuez, A.; Romero, F. M.; Rusanov, E.; Stoeckli-Evans, H. *Inorg. Chem.* **2002**, *41*, 4615. (h) Andrés, R.; Brissard, M.; Gruselle, M.; Train, C.; Vaissermann, J.; Malézieux, B.; Jamet, J.-P.; Verdaguer, M. *Inorg. Chem.* **2001**, *40*, 4633.
(8) (a) Ohkoshi, S.; Shimura, J.; Ikeda, K.; Hashimoto, K. *J. Opt. Soc. Am. B* **2005**, *22*, 196. (b) Tsunobuchi, Y.; Kosaka, W.; Nuida, T.; Ohkoshi, S. *CrystEngComm.* **2009**, *11*, 2051–2053. (c) Train, C.; Nuida, T.; Gheorghe, R.; Gruselle, M.; Ohkoshi, S. *J. Am. Chem. Soc.* **2009**, *131*, 16838–16843.

Published on Web 12/09/2010

second harmonic generation (MSHG)[8a] in noncentrosymmetric[8b] and chiral ones.[8c] Such materials can be realized from either achiral components giving rise to a molecular magnet crystallizing in a noncentrosymmetric[8b] and chiral space group[9] or rationally, through the use of chiral building blocks (ligands).[7]

Recently, octacyanidometalate $[M(CN)_8]^{3-/4-}$ anions (M = Nb(IV), Mo(IV,V), and W(IV,V) attract much attention as suitable building blocks for the construction of promising 4Ms. The presence of eight cyanido ligands in $[M(CN)_8]^{3-/4-}$, which can potentially form up to eight molecular bridges to paramagnetic 3d and 4f metal centers, allows for the construction of molecular magnets exhibiting full spectrum of coordination topologies.[10] The topology of the resulting $[M(CN)_8]$-based network can be easily controlled by the introduction of additional molecules acting as guest, blockers, linkers, or spacers. Rational combination of carefully selected building blocks (cationic metal centers, organic/inorganic molecules) influences not only the topology-related physicochemical properties like porosity but allows for introduction of additional functionalities, because each building block can be a prerequisite for additional property. This approach has afforded recently new fascinating examples of $[M(CN)_8]$-based magnets:[10−21] light or solvent tunable ones,[11−13,15,18] magnets showing spin isomerism[15,20] and high-temperature magnets[21] with T_c up to 138 K. Octacyanidometalates, however, have been very scarcely used for the construction of noncentrosymmetric or chiral magnets. There are just two examples of isomorphic pyroelectric hybrid compounds based on Mn^{II}-$[Mo^{IV}(CN)_8]^{4-}$[21,22a] and Mn^{II}-$[Nb^{IV}(CN)_8]^{4-}$[7,8a,22b] of which the latter shows also ferrimagnetic ordering below 48 K and belongs therefore to the class of multiferroics.[23] To the best of our knowledge, just two examples of $[M(CN)_8]$-based compounds show chirality: paramagnetic $Ni^{II}-Mo^{IV}$ coordination polymer[9c] self-assembled from achiral building blocks and antiferromagnetic $\{[W(CN)_8]_4[Cu((S\text{-or-}R)\text{-pn})H_2O]_4[Cu((S\text{-or-}R)\text{-pn})]_2\cdot 2.5H_2O\}$[24] rationally synthesized using enantiomerically pure (S-or-R)-1,2-diaminopropane ((S-or-R)-pn) as a blocking ligand.

To obtain novel noncentrosymmetric molecular magnet, we have focused on the molecular design of the 4M incorporating urea, the efficient nonlinear optical (NLO) material,[25a] into magnetic Mn^{II}-$[Nb(CN)_8]^{4-}$ 3D coordination network. Urea molecules exhibit large molecular first hyperpolarizability and can give rise to very interesting NLO materials with very large second-order susceptibilities if properly oriented in a noncentrosymmetric crystal lattice. Urea can be used as a dopant[25c] or as one of the components of mixed organic crystals[25b] enhancing the optical properties of NLO materials. In this paper, we report the successful isolation of two novel urea-based $\{[Mn^{II}(H_2O)(urea)_2]_2[Nb^{IV}(CN)_8]\}_n$ polymorphs: noncentrosymmetric **α** and centric β crystallizing in space group $P4_1$ and $P\bar{1}$, respectively. Both phases exhibit transition to the magnetically ordered state below 43 and 42 K, respectively, but only in case of polymorph α, incorporation of urea molecules coordinated to Mn^{II} centers and arranged in a noncentrosymmetric molecular pattern produces additional functionality: second harmonic generation (SHG). Below magnetic transition temperature T_c both funtionalities interact with each other producing MSHG, a second-order NLO effect, known also as nonlinear magneto-optical Kerr effect (NOMOKE).

The subtle structural differences between both polymorphs that control their overall symmetry and result in the emergence of NLO behavior in α do not influence their complex reactivity. In methanol, both polymorphs release urea from their structures and transform into the same amorphous solid $\{[Mn^{II}(H_2O)]_2[Nb^{IV}(CN)_8]\cdot xMeOH\}_n$ (MeOH = methanol) **2a** and subsequently $\{[Mn^{II}(H_2O)]_2[Nb^{IV}(CN)_8]\cdot 2.5MeOH\}_n$ **2b** with significant shift of critical temperature T_c to the value of 70 K. If compound **2b** is exposed to water vapors, it transforms further into $\{[Mn^{II}(H_2O)_2]_2[Nb^{IV}(CN)_8]\cdot 4H_2O\}_n$ **3** reported recently by Herrera et al.[26] with T_c of 47 K. In water, both α and β can be turned directly into **3**.

(9) (a) Gao, E.-Q.; Yue, Y.-F.; Bai, S.-Q.; He, Z.; Yan, Ch.-H. *J. Am. Chem. Soc.* **2004**, *126*, 1419. (b) Paredes-García, V.; Vega, A.; Novak, M. A.; Vaz, M. G. F.; Souza, D. A.; Venegas-Yazigi, D.; Spodine, E. *Inorg. Chem.* **2009**, *48*, 4737–4742. (c) Zhang, W.; Wang, Z.-Q.; Sato, O.; Xiong, R.-G. *Cryst. Growth Des.* **2009**, *9*, 2050–2053.

(10) Przychodzeń, P.; Korzeniak, T.; Podgajny, R.; Sieklucka, B. *Coord. Chem. Rev.* **2006**, *250*, 2234.

(11) Ohkoshi, S.; Tokoro, H.; Hozumi, T.; Zhang, Y.; Hashimoto, K.; Mathoniere, C.; Bord, I.; Rombaut, G.; Verelst, M.; Cartier dit Moulin, Ch.; Villain, F. *J. Am. Chem. Soc.* **2006**, *128*, 270.

(12) Ohkoshi, S.; Tsunobuchi, Y.; Takahashi, H.; Hozumi, T.; Shiro, M.; Hashimoto, K. *J. Am. Chem. Soc.* **2007**, *129*, 3084.

(13) Nowicka, B.; Rams, M.; Stadnicka, K.; Sieklucka, B. *Inorg. Chem.* **2007**, *46*, 8123.

(14) Podgajny, R.; Chmel, N. P.; Bałanda, M.; Tracz, P.; Gaweł, B.; Zając, D.; Sikora, M.; Kapusta, Cz.; Łasocha, W.; Wasiutyński, T.; Sieklucka, B. *J. Mater. Chem.* **2007**, *17*, 3308.

(15) (a) Le Bris, R.; Mathonière, C.; Letard, J.-F. *Chem. Phys. Lett.* **2006**, *426*, 380. (b) Ohkoshi, S.; Hamada, Y.; Matsuda, T.; Tsunobuchi, Y.; Tokoro, H. *Chem. Mater.* **2008**, *20*, 3048.

(16) Podgajny, R.; Pinkowicz, D.; Korzeniak, T.; Nitek, W.; Rams, M.; Sieklucka, B. *Inorg. Chem.* **2007**, *46*, 10416.

(17) Pinkowicz, D.; Podgajny, R.; Nitek, W.; Makarewicz, M.; Czapla, M.; Mihalik, M.; Bałanda, M.; Sieklucka, B. *Inorg. Chim. Acta* **2008**, *361*, 3957.

(18) Pinkowicz, D.; Podgajny, R.; Bałanda, M.; Makarewicz, M.; Gaweł, B.; Łasocha, W.; Sieklucka, B. *Inorg. Chem.* **2008**, *47*, 9745.

(19) Kosaka, W.; Hashimoto, K.; Ohkoshi, S. *Bull. Chem. Soc. Jpn.* **2008**, *81*, 992.

(20) Arai, M.; Kosaka, W.; Matsuda, T.; Ohkoshi, S. *Angew. Chem., Int. Ed.* **2008**, *47*, 6885.

(21) Kosaka, W.; Imoto, K.; Tsunobuchi, Y.; Ohkoshi, S. *Inorg. Chem.* **2009**, *48*, 4604.

(22) (a) Kosaka, W.; Nuida, T.; Hashimoto, K.; Ohkoshi, S. *Bull. Chem. Soc. Jpn.* **2007**, *80*, 960–962. (b) Kosaka, W.; Hashimoto, K.; Ohkoshi, S. *Bull. Chem. Soc. Jpn.* **2008**, *81*, 992–994.

(23) (a) Khomski, D. *Physics* **2009**, *2*, 20. (b) Spaldin, N. A.; Fiebig, M. *Science* **2005**, *309*, 391–392. (c) Eerenstein, W.; Mathur, N. D.; Scott, J. F. *Nature* **2006**, *442*, 759–765.

(24) Higashikawa, H.; Okuda, K.; Kishine, J.-I.; Masuhara, N.; Inoue, K. *Chem. Lett.* **2007**, *36*, 1022–1023.

(25) (a) Donaldson, W. R.; Tang, C. L. *Appl. Phys. Lett.* **1984**, *44*, 25–27. (b) Lin, Y. Y.; Rajesh, N. P.; Santhana Raghavan, P.; Ramasamy, P.; Huang, Y. C. *Mater. Lett.* **2002**, *56*, 1074–1077. (c) Bhagavannarayana, G.; Kushwaha, S. K. *J. Appl. Crystallogr.* **2010**, *43*, 154–162.

(26) (a) Herrera, J. M.; Franz, P.; Podgajny, R.; Pilkington, M.; Biner, M.; Decurtins, S.; Stoeckli-Evans, H.; Neels, A.; Garde, R.; Dromzée, Y.; Julve, M.; Sieklucka, B.; Hashimoto, K.; Ohkoshi, S.; Verdaguer, M. *C. R. Chimie* **2008**, *11*, 1192–1199. (b) Pilkington, M.; Decurtins, S. *Chimia* **2000**, *54*, 593.

(27) Kiernan, P. M.; Griffith, W. P. *J. Chem. Soc., Dalton Trans.* **1975**, 2489.

2. Experimental Section

2.1. Materials. Chemicals and solvents used in this study were purchased from commercial sources (Fluka, Aldrich) and used without further purification. Potassium octacyanoniobate-(IV) dihydrate $K_4[Nb(CN)_8]\cdot 2H_2O$ was prepared according to literature procedures.[27]

2.2. Synthesis of the Chiral Polymorph $\{[Mn^{II}(urea)_2(H_2O)]_2[Nb^{IV}(CN)_8]\}_n$ α. $MnCl_2\cdot 4H_2O$ (1.0 mmol, 197 mg) and urea (33.3 mmol, 2000 mg) were dissolved in 5.0 mL of distilled water and added to an aqueous solution of $K_4Nb(CN)_8\cdot 2H_2O$ (0.2 mmol, 99 mg, 2.0 mL). The resulting yellow solution was left to stand in the dark for 72 h without filtration. Large ($1.5 \times 1 \times 1$ mm^3) red block crystals were collected and washed with small portions of ethanol and dried in air (yield ~40%). Large single crystals of α are air-stable for several months. Anal. Calcd for $C_{12}H_{20}Mn_2N_{16}NbO_6$: C, 20.97; H, 2.93; N, 32.61. Found: C, 21.09; H, 2.83; N, 32.18. IR (KBr) in cm^{-1}: ν(N−H) 3496 vs; ν(O−H) 3406vs; ν(C≡N) 2158w, 2151 m, 2135s; ν(C═O) 1632vs; γ(N−H) 1574vs; ν(C−N) 1488s; ν(Nb−C) 463s. Pure chiral α was also obtained in form of a fine powder by stirring the reaction mixture for about 20 h.

2.3. Synthesis of the Centric Polymorph $\{[Mn^{II}(urea)_2(H_2O)]_2[Nb^{IV}(CN)_8]\}_n$ β. $MnCl_2\cdot 4H_2O$ (1.0 mmol, 197 mg) and urea (33.3 mmol, 2500 mg) were dissolved in 3.5 mL of distilled water and added to an aqueous solution of $K_4Nb(CN)_8\cdot 2H_2O$ (0.2 mmol, 99 mg, 0.5 mL). The resulting yellow solution was filtered and left to stand in the dark for 24 h. After this time the solution was filtered once again and left for another 24 h. Orange platelike crystals were collected and washed with small portions of ethanol and dried in air (yield ~30%). Anal. Calcd for $C_{12}H_{20}Mn_2N_{16}NbO_6$: C, 20.97; H, 2.93; N, 32.61. Found: C, 20.62; H, 2.98; N, 32.25. IR (KBr) in cm^{-1}: ν(N−H) 3496 vs; ν(O−H) 3407vs; ν(C≡N) 2157w, 2151 m, 2135s; ν(C═O) 1635vs; γ(N−H) 1573vs; ν(C−N) 1488s; ν(Nb−C) 462s. Pure chiral β was also obtained in form of fine powder by stirring the reaction mixture for about 4 h.

2.4. Preparation of $\{[Mn^{II}(H_2O)]_2[Nb^{IV}(CN)_8]\cdot xMeOH\}_n$ 2a and $\{[Mn^{II}(H_2O)]_2[Nb^{IV}(CN)_8]\cdot 2.5MeOH\}_n$ 2b. Red single crystals of $\{[Mn^{II}(urea)_2(H_2O)]_2[Nb^{IV}(CN)_8]\}_n$ α were crushed and placed in methanol. After about 24 h the color change from red to yellow was observed. The yellow product $\{[Mn^{II}(H_2O)]_2[Nb^{IV}(CN)_8]\cdot xMeOH\}_n$ **2a** was filtered and dried very briefly in air. Elemental analyses for three independently prepared samples of **2a** showed the presence of variable number of methanol molecules per formula unit (between 3.5 and 5). Average Anal. Calcd for $C_{12}H_{20}Mn_2N_8NbO_6$ ($x = 4$): C, 25.06; H, 3.51; N, 19.48. Found: C, 24.48; H, 3.31; N, 19.76. IR (KBr) in cm^{-1}: ν(O−H) 3564vs; ν(C≡N) 2145vs (with shoulder at 2160); γ(O−H) 1609s; ν(C−O) 1004w, 977 m; ν(Nb−C) 476vs Drying of **2a** in vacuo for about 10 min over P_2O_5 leads to compound $\{[Mn^{II}(H_2O)]_2[Nb^{IV}(CN)_8]\cdot 2.5MeOH\}_n$ **2b** with stable content of methanol. Anal. Calcd for $C_{10.5}H_{14}Mn_2N_8NbO_{4.5}$: C, 23.93; H, 2.68; N, 21.26. Found: C, 23.76; H, 2.60; N, 21.15. IR (KBr) in cm^{-1}: ν(O−H) 3602vs; ν(C≡N) 2144vs (broad); γ(O−H) 1614vs; ν(C−O) 1000w (broad); ν(Nb−C) 474vs. **2a** and **2b** can be also obtained from β utilizing the same procedure.

2.5. Preparation of $\{[Mn^{II}(H_2O)_2]_2[Nb^{IV}(CN)_8]\cdot 4H_2O\}_n$ 3. Yellow powder of **2b** was placed in a closed vessel filled with water vapors. Within a few minutes, color change from yellow to red was observed and crystalline product **3** was formed. **3** is stable under ambient conditions. Anal. Calcd for $C_8H_{16}Mn_2N_8NbO_8$: C, 17.31; H, 2.91; N, 20.19. Found: C, 17.76; H, 2.40; N, 19.57. IR (KBr) in cm^{-1}: ν(O−H) 3569vs; ν(C≡N) 2151s, 2141vs; γ(O−H) 1613s; ν(Nb−C) 472s, 444 m.

2.6. Structure Solution and Refinement. The single-crystal diffraction data were collected at room temperature on a Nonius Kappa CCD diffractometer equipped with a Mo Kα radiation source and graphite monochromator. The space group was determined using ABSEN.[28] Structures of both polymorphs α and β were solved by direct methods using SIR-97.[29] Refinement and further calculations were carried out using SHELXL-97.[30] The non-H atoms were refined anisotropically using weighted full-matrix least-squares on F^2. Hydrogen atoms were unreachable. The structure of α was refined as twinned with twin law [−1 0 0 0 −1 0 0 0 −1]. The final Flack parameter for α was equal to 0.67(4). Such value in case of enatiomorphic space group $P4_1$ indicates racemic twinning but with significant dominance of $P4_3$ enantiomorph. Selected crystallographic data for α and β are shown in Table SI-1 in the Supporting Information. In the case of β, the values of R_1 and wR_2 indices are high because of the low quality of obtained crystals. All attempts to obtain better ones were unsuccessful. Structural diagrams were prepared using Mercury 1.4.2, VESTA,[31] Ortep32,[32] or POV-Ray[33] software.

2.7. X-ray Powder Diffraction (XRPD) Measurements. XRPD patterns of powders of α and β were recorded at room temperature on D8 Advance Bruker diffractometer (CuKα radiation) with 0.02° step in the 5−70° 2θ range. XRPD patterns of **2b** and **3** were recorded at room temperature in 5−120° 2θ range (continuous scan mode) on Panalytical X'PERT PRO (CuKα radiation) equipped with X'Celerator solid state detector.

2.8. MSHG Measurements. For MSHG measurements, the incident light was provided by an optical parametric amplifier (Clark-MXR Vis-OPA; pulse width, 190 fs; repetition, 1 kHz) pumped by a frequency-doubled Ti:sapphire laser (Clark-MXR CPA-2001; wavelength, 775 nm; pulse width, 150 fs; repetition, 1 kHz). The reflected SHG light was detected by a photomultiplier tube (Hamamatsu R329−02) through color filters. The temperature of the samples was controlled using a cryostat (Daikin PS22). The basal plain of the single crystal α was mounted in the cryostat and we take the x, y, and z axes parallel to the a, b, and c axes of the crystal as shown in the Figure 1. The angle of incidence and reflection on the sample was fixed at 30°. The polarization of the incident light is kept p-polarized. The magnetic field of 500 Oe was applied along the a-axis using permanent magnets.

2.9. Other Physical Measurements. Elemental analyses (C, H, N) were performed using an Elementar vario MICRO cube elemental analyzer. Infrared spectra were measured in KBr pellets between 4000 and 400 cm^{-1} using a Bruker EQUINOX 55 FT-IR spectrometer. Magnetization measurements were performed using Quantum Design SQUID magnetometer MPMS5-XL. Magnetic measurements for **2a** were carried out in a tightly closed sample holder filled with methanol. Magnetic measurements for **2b** were carried out in a tightly closed sample holder after 10 min of drying in vacuo over phosphorus pentoxide (these sample holders were adapted from Lakeshore 7225 susceptometer).

2.10. Calculations. Continuous Shape Measure Analysis for coordination spheres of Mn^{II} and Nb^{IV} in α and β was performed with use of SHAPE software ver. 1.1b.[35] The details of

(28) McArdle, P. *J. Appl. Crystallogr.* **1996**, *29*, 306.
(29) Altomare, A.; Burla, M. C.; Camalli, M.; Cascarano, G. L.; Giacovazzo, C.; Guagliardi, A.; Moliterni, A. G. G.; Polidori, G.; Spagna, R. *J. Appl. Crystallogr.* **1999**, *32*, 115.
(30) Sheldrick, G. M. *Acta Crystallogr.* **2008**, *A64*, 112–122.
(31) Momma, K.; Izumi, F. *Commission on Crystallogr. Comput., IUCrNewslett* **2006**, 7, 106.
(32) Farrugia, L. J. *J. Appl. Crystallogr.* **1997**, *30*, 565.
(33) Persistence of Vision Raytracer (Version 3.6); Persistence of Vision Pty. Ltd: Farnham, Surrey, U.K., 2004; retrieved from http://www.povray.org/download/.
(34) (a) Kahn, O. *Molecular Magnetism*; Wiley-VCH: Weinheim, Germany, 1993; pp 3−4. (b) Néel, L. *Ann. Phys.* **1948**, *137*, 137–198.

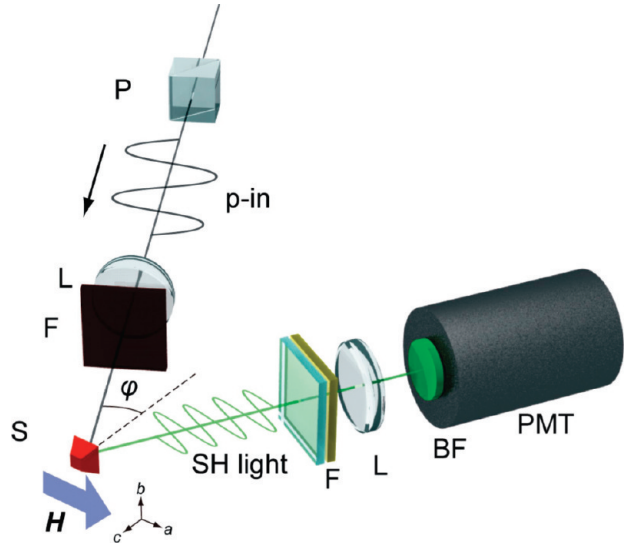

Figure 1. Schematic illustration of experimental set up for MSHG measurements (P, polarizer; L, lens; F, color filter; S, single crystal of α; BF, bandpass filter; PMT, photomultiplier tube).

the analysis can be found in the Supporting Infomation, paragraph 2.

3. Results and Discussion

3.1. Characterization and Reactivity of α and *β*. *Structural Characterization of* α *and* β. Self-assembly of Mn^{2+} cations with $[Nb(CN)_8]^{4-}$ anions in a highly concentrated aqueous solution of urea leads to the formation of two $\{[Mn^{II}(urea)_2(H_2O)]_2[Nb^{IV}(CN)_8]\}_n$ crystal polymorphs α and β which crystallize in chiral $P4_1$ and centric $P\bar{1}$ space group, respectively. Synthesis of the specific polymorph can be very easily controlled by the overall concentration of the mother liquor. Single crystals of the chiral α can be obtained from slightly more diluted solutions than the crystals of the β form. Single-crystal X-ray diffraction on both polymorphs revealed exceptional structural similarity. Both α and β exhibit identical 3D coordination framework based on cyanido-bridges linking Mn^{II} and Nb^{IV} centers. Their 3D coordination skeletons can be described as comprising two sets of infinite waved ladder-motifs running along *a* and *b* direction respectively and cross-linking at Nb^{IV} centers (Figure 2a,b). Although Nb atoms link both ladders' sets together, giving rise to the 3D coordination network, Mn atoms belong exclusively to one of the sets. The difference between α and β manifests itself in the mutual arrangement of the ladder-motifs of the same type: herringbone-like in α and parallel in β. Figure 2c,d shows almost perfectly identical local fragments of both polymorphic structures with atom labeling schemes.

Coordination sphere of Nb^{IV} centers in α (Figure 2c,d) is dodecahedral according to the results of continuous shape measure (CShM) analysis (with S_4 axis aligned parallel to the crystallographic *c* direction; paragraph 2 in the Supporting Information) and is composed of eight carbon atoms of eight CN^- ligands. Six cyanido ligands act as molecular bridges forming $Nb^{IV}-CN-Mn^{II}$ linkages and the remaining two are terminal ones. The CShM Analysis for coordination spheres of Mn^{II} in form α (paragraph 2 in the Supporting Information) shows that both Mn1 and Mn2 exhibit distorted octahedral geometry. Both coordination spheres consist of three nitrogen atoms of bridging cyanido ligands in *mer* geometry, two oxygen atoms of two monodentate urea molecules in *cis* geometry, and one oxygen atom of aqua ligand (Figure 2c, d, respectively). The presence of six and three bridging cyanides per Nb^{IV} and Mn^{II}, respectively, results in 6:3 connectivity type (see Figure SI-1 in the Supporting Information). Coordination spheres in β are very similar but slightly more distorted (according to CShM analysis; paragraph 2 in the Supporting Information) and the connectivity type is identical.

Table 1 shows selected interatomic distances and angles of both polymorphs. All parameters of the Nb−CN−Mn linkages are remarkably similar, supporting the previous statement that the local fragments of both structures are identical. The average $Nb-C_{cyanido}$ distances in α and β are 2.25(3) and 2.25(2) Å, respectively, the average $Mn1-N_{cyanido}$ bond lengths are α, 2.19(7) Å; β, 2.19 (6) Å; and $Mn2-N_{cyanido}$ bond lengths are α, 2.20(3) Å; β, 2.20(5) Å. The Mn−N−C angles are also very similar: 162(9) for α and 163(10) for β. Identical geometry of the Nb−CN−Mn linkages produces consequently identical Mn···Nb distances. Their average values are equal for both polymorphs, 5.52(12) Å. Metric parameters of α and β are comparable with those reported previously for $Mn^{II}-Nb^{IV}(CN)_8$-based coordination compounds.[10,16−19]

Both cyanido-frameworks can be described alternatively as consisting of interconnected parallel Mn_2Nb cyanido-chains running along *c* axis. In both compounds the chains are built of rhomboid Mn_2Nb_2 units sharing Nb-corners (−C1N1−, −C2N2−, −C5N5−, and −C7N7− in α and −C2N2−, −C5N5−, −C6N6−, and −C7N7− in β) and are interconnected by the remaining two cyanido-bridges. The difference between α and β consists in the arrangement of the rhomboid Mn_2Nb_2 units forming homochiral helical chains in polymorph α and nonchiral zigzag chains in β (see Figure SI-2 in the Supporting Information).

Cyanido-bridged frameworks of α and β are very effectively stabilized by the presence of hydrogen bonds between nitrogen and oxygen atoms of neighboring urea molecules (ca. 3.0 Å for both polymorphs; see Figure SI-3a in the Supporting Information), between oxygen atoms of aqua ligands, oxygen atoms of urea (ca. 2.9 Å), nitrogen atoms of urea (ca. 3.0 Å), and nitrogen atoms of terminal cyanido ligands (ca. 2.9 Å; see Figure SI-3b in the Supporting Information). The presence of direct hydrogen bonds between oxygen atoms of aqua ligands of both Mn^{II} centers

(35) (a) Llunell, M.; Casanova, D.; Cirera, J.; Bofill, J. M.; Alemany, P.; Alvarez, S.; Pinsky, M.; Avnir, D. SHAPE v. 1.1b. Program for the Calculation of Continuous Shape Measures of Polygonal and Polyhedral Molecular Fragments; University of Barcelona: Barcelona, Spain, 2005. (b) Casanova, D.; Cirera, J.; Llunell, M.; Alemany, P.; Avnir, D.; Alvarez, S. *J. Am. Chem. Soc.* **2004**, *126*, 1755. (c) Alvarez, S.; Alemany, P.; Casanova, D.; Cirera, J.; Llunell, M.; Avnir, D. *Coord. Chem. Rev.* **2005**, *249*, 1693. (d) Casanova, D.; Llunell, M.; Alemany, P.; Alvarez, S. *Chem.—Eur. J.* **2005**, *11*, 1479. (f) Cirera, J.; Ruiz, E.; Alvarez, S. *Chem.—Eur. J.* **2006**, *12*, 3162.

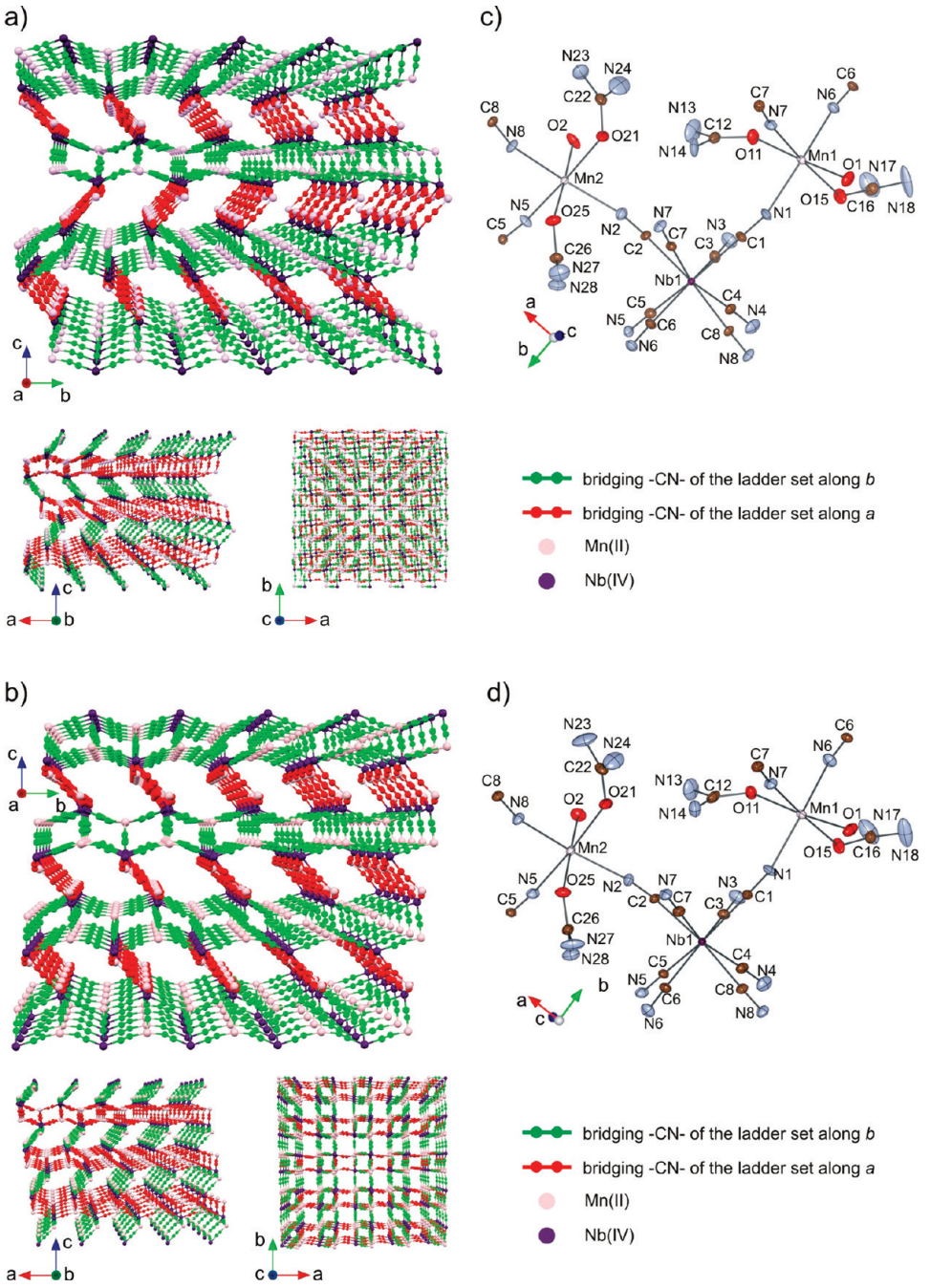

Figure 2. Packing diagrams of (a) α and (b) *β* showing unusual similarity of their 3D coordination skeletons and the difference in the mutual arrangement of ladder motifs: herringbone-like in α and parallel in *β* (urea, terminal cyanides, and aqua ligands omitted for clarity); identical "local" fragments of the structures of (c) α and (d) *β*.

and respective nitrogen atoms of both terminal cyanido ligands of Nb^{IV} (dashed red lines in Figure SI-3b in the Supporting Information) leads to the possible path for topological formation of additional two Nb−CN−Mn linkages in case of breaking of these hydrogen bonds.

PXRD patterns of both $\{[Mn^{II}(urea)_2(H_2O)]_2[Nb^{IV}(CN)_8]\}_n$ polymorphs obtained in form of fine powders are presented in Figure 3. The respective calculated patterns fit well the experimental ones indicating that structural models obtained from single-crystal XRD experiments are valid for bulk samples. IR spectra of both α and *β* (see Figure SI-4 in the Supporting Information with the detailed description) are identical and confirm the presence of bridging cyanido ligands[10] and coordinated urea molecules.[36]

Reactivity of α *and* *β*. Both polymorphic forms of the $\{[Mn^{II}(urea)_2(H_2O)]_2[Nb^{IV}(CN)_8]\}_n$ system exhibit very similar reactivity, which is summarized in Scheme 1. In methanol α and *β* transform into the same amorphous compound $\{[Mn^{II}(H_2O)]_2[Nb^{IV}(CN)_8]\cdot x\text{MeOH}\}_n$ **2a** replacing four urea ligands with methanol molecules. **2a** loses MeOH extremely easy, which might be the reason for its amorphous character. Drying of **2a** in vacuo over phosphorus

(36) Socrates, G. *Infrared Characteristic Group Frequencies*; John Wiley & Sons: New York, 1994.

Table 1. Selected Interatomic Distances and Angles in α and *β* (average values with standard deviation in parentheses are bolded)

	coordination spheres of Nb (Å)		coordination spheres of Mn (Å)			
	α	*β*	α		*β*	
Nb−C1	2.238(7)	2.231(8)	Mn1−N1	2.149(6)	Mn1−N1	2.153(8)
Nb−C2	2.230(6)	2.236(8)	Mn1−N6	2.143(6)	Mn1−N6	2.159(8)
Nb−C3	2.259(8)	2.270(9)	Mn1−N7	2.272(6)	Mn1−N5	2.264(8)
Nb−C4	2.267(7)	2.267(9)	Mn1−O1	2.232(6)	Mn1−O1	2.210(7)
Nb−C5	2.264(6)	2.291(9)	Mn1−O11	2.244(6)	Mn1−O11	2.277(7)
Nb−C6	2.235(7)	2.227(8)	Mn1−O15	2.219(5)	Mn1−O15	2.206(7)
Nb−C7	2.300(7)	2.268(8)	Mn2−N2	2.182(6)	Mn2−N2	2.177(8)
Nb−C8	2.222(6)	2.239(9)	Mn2−N8	2.180(5)	Mn2−N8	2.164(8)
avg Nb−C	**2.252(26)**	**2.254(23)**	Mn2−N5	2.230(6)	Mn2−N7	2.250(8)
			Mn2−O2	2.230(6)	Mn2−O2	2.214(7)
			Mn2−O21	2.207(6)	Mn2−O21	2.191(7)
			Mn2−O25	2.243(5)	Mn2−O25	2.255(7)
			avg Mn1−N	**2.188(73)**	**avg Mn1−N**	**2.192(62)**
			avg Mn2−N	**2.197(28)**	**avg Mn2−N**	**2.197(46)**

	Mn···Nb distance (Å)		C−N−Mn angles (deg)			
	α	*β*	α		*β*	
Nb−C1−N1−Mn1	5.423(15)	5.436(20)	C1−N1−Mn1	154.3(7)	C1−N1−Mn1	155.6(8)
Nb−C2−N2−Mn2	5.411(15)	5.401(20)	C6−N6−Mn1	164.2(7)	C6−N6−Mn1	164.1(8)
Nb−C5−N5−Mn2	5.660(15)		C7−N7−Mn1	172.8(6)	C7−N7−Mn2	173.1(8)
Nb−C5−N5−Mn1		5.694(20)	C2−N2−Mn2	150.3(6)	C2−N2−Mn2	150.7(8)
Nb−C6−N6−Mn1	5.469(15)	5.487(20)	C8−N8−Mn2	162.1(6)	C8−N8−Mn2	163.2(8)
Nb−C7−N7−Mn1	5.664(15)		C5−N5−Mn2	173.5(6)	C5−N5−Mn1	175.2(8)
Nb−C7−N7−Mn2		5.657(20)	**avg C−N−Mn**	**162(9)**	**avgC−N−Mn**	**163(10)**
Nb−C8−N8−Mn2	5.473(15)	5.478(20)				
avg Nb···Mn	**5.52(12)**	**5.53(12)**				

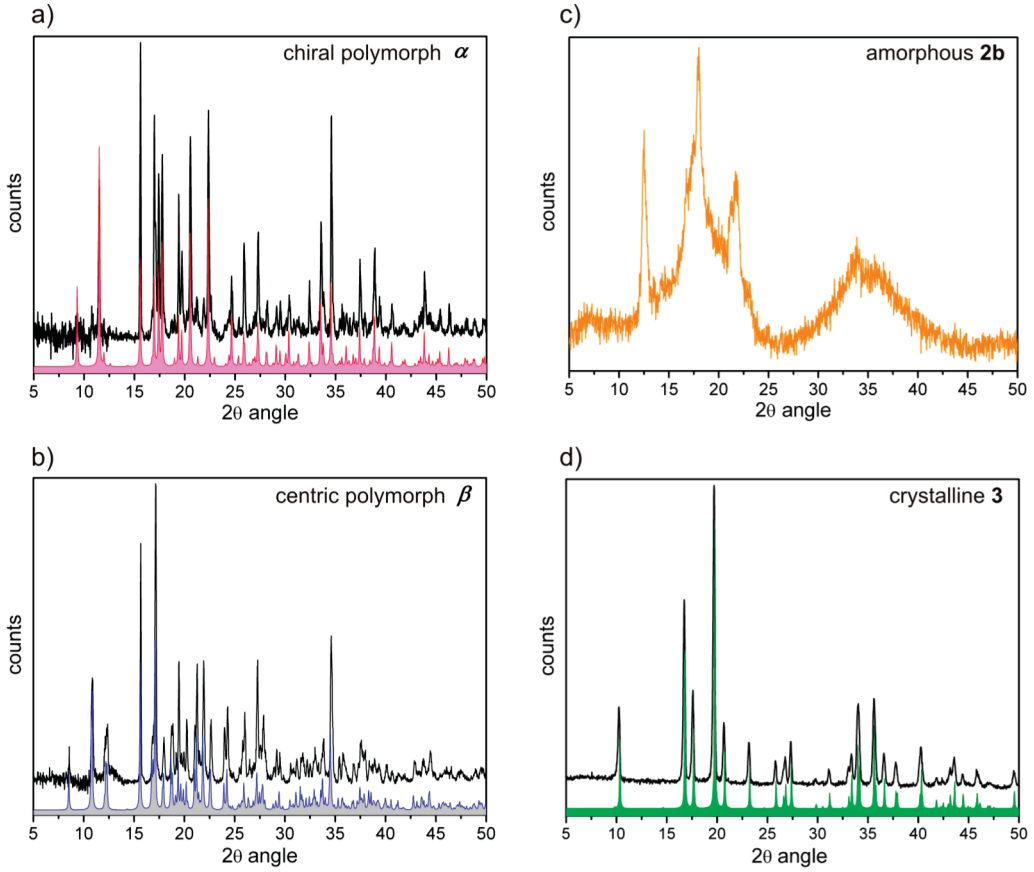

Figure 3. PXRD patterns of compounds: (a) α, (b) *β*, (c) **2b**, and (d) **3.** In a, b, and d, black solid lines are the experimental patterns and color lines are the respective calculated patterns from single-crystal XRD models.

pentoxide leads to a stable amorphous phase $\{[Mn^{II}(H_2O)]_2[Nb^{IV}(CN)_8]\cdot 2.5MeOH\}_n$ **2b** with reduced number of MeOH molecules per formula unit. **2b** is extremely sensitive to humidity and in the presence of water vapors

Scheme 1. Reactivity of $\{[Mn^{II}(urea)_2(H_2O)]_2[Nb^{IV}(CN)_8]\}_n$ System

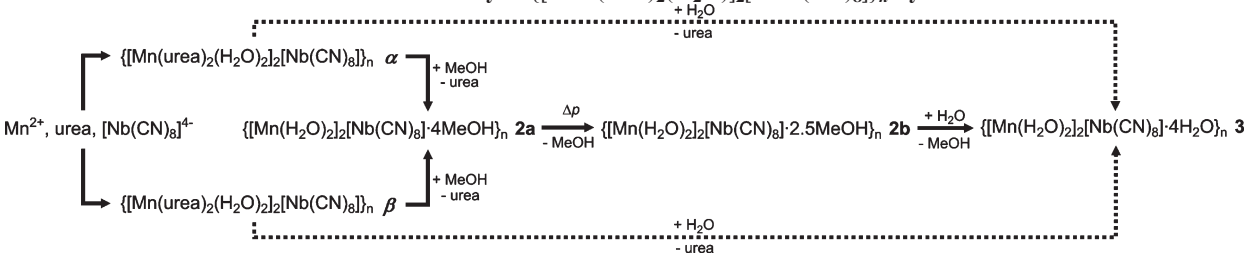

transforms into crystalline $\{[Mn^{II}(H_2O)_2]_2[Nb^{IV}(CN)_8]\cdot 4H_2O\}_n$ **3**.[26] This $\alpha/\beta \rightarrow$ **2a** $\rightarrow$ **2b** $\rightarrow$ **3** transformation path is indicated in the scheme by solid arrows. In water, solid samples of α/β undergo subsequent dissolution and immediate recrystallization into **3** (dashed arrows in the scheme). The transformations and their products **2a**, **2b**, and **3** were investigated with PXRD and IR spectroscopy.

In methanol, the red/orange crystals of α/β change their color to yellow. The resulting product $\{[Mn^{II}(H_2O)]_2[Nb^{IV}(CN)_8]\cdot 4MeOH\}_n$ **2a** keeps the shape of the parent crystals, but loses its crystallinity. The PXRD pattern of **2** has strongly amorphous character (Figure 3c), which prevents its structural characterization using diffraction methods. Elemental analysis of the stable phase **2b** leads to the chemical formula with two and a half methanol molecules per formula unit. The role of methanol in the structure, however, is not well recognized. We assume that it might be bound very weakly and might be the major cause of the amorphous character of **2a** and **2b**. The IR spectra (Figure SI-4 in the Supporting Information) shows some significant changes in comparison to α and β. The bands characteristic for coordinated urea completely disappear and characteristic bands of methanol appear. The ν(C≡N) band is shifted toward higher values than the corresponding ones in α and β. These two observations suggest the formation of additional Nb−CN−Mn linkages in compound **2b**.[5f,g,18]

When exposed to moisture, yellow amorphous **2b** transforms rapidly into red crystalline **3**, losing all remaining methanol molecules. The PXRD pattern of **3** (Figure 3d) fits perfectly that of $\{[Mn^{II}(H_2O)_2]_2[Nb^{IV}(CN)_8]\cdot 4H_2O\}_n$.[26] IR spectrum of **3** (see Figure SI-4 in the Supporting Information) supports its PXRD identification as $\{[Mn^{II}(H_2O)_2]_2[Nb^{IV}(CN)_8]\cdot 4H_2O\}_n$. Compound **3** crystallizes in centrosymmetric tetragonal space group $I4/m$ and is a 3D cyanido-bridged coordination polymer. Its skeleton consists of perpendicular sets of corrugated square-grids cross-linking at niobium(IV) centers (Figure 4). In the coordination sphere of Nb^{IV} square antiprism, there are eight *C*-coordinated cyanido ligands, which form molecular bridges to eight Mn^{II} centers. Each octahedral Mn^{II} is connected through four equatorially positioned *N*-coordinated cyanido ligands to four Nb^{IV} centers. Remaining axial positions of the octahedral sphere of Mn^{II} are occupied by two water molecules. The existence of eight and four bridging cyanides per Nb^{IV} and Mn^{II}, respectively, gives rise to 8:4 connectivity type. The increase of the connectivity from 6:3 for α/β to 8:4 in **3** can be explained in terms of the topological formation of additional Nb-CN-Mn linkages, when the coordination sites at Mn-centers of α/β become available upon release of blocking urea ligands in the intermediate compound **2b**.

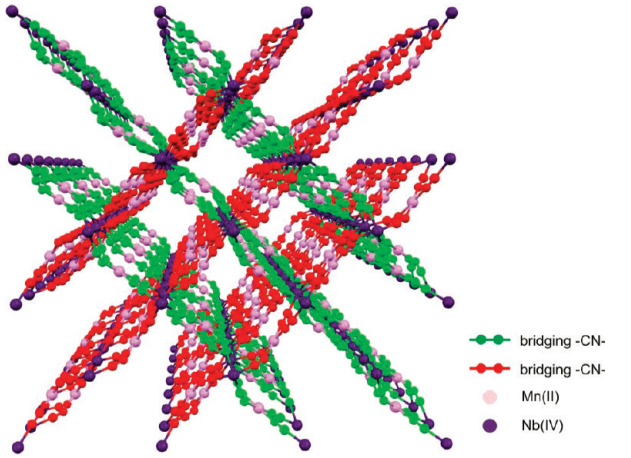

Figure 4. Packing diagram of **3** showing its 3D skeleton consisting of perpendicular sets of corrugated square-grids cross-linking at niobium(IV) centers (aqua ligands omitted for clarity).

The IR and EA characteristics of **2b** together with its role of intermediate species between α/β and **3** in the α/β $\rightarrow$ **2b** $\rightarrow$ **3** transformation sequence suggest that it exhibits 8:4 connectivity type, with eight bridging cyanido ligands per formula unit and molecules of methanol filling the empty spaces. Figure SI-5 (Supporting Information) shows the consecutive structural changes in the $\alpha/\beta \rightarrow$ **2b** $\rightarrow$ **3** transformation sequence (**2a** is omitted for clarity) and the proposed structure of **2b** with methanol filling the voids in the cyanido-skeleton. Both stages of the transformation are completely irreversible. The possible reason for the irreversibility of the first stage $\alpha/\beta \rightarrow$ **2a** $\rightarrow$ **2b** is the direct ("easy") topotactic pathway for the formation of two Nb-CN-Mn linkages per formula unit (with the relatively short $Mn^{II}\cdots N_{terminalCN}$ initial distance of 4.6 Å) and large structural contraction upon removal of bulky urea ligands in α/β so their reabsorption is completely hindered. In comparison to this, similar topotactic changes in the magnetic spongelike system $\{Mn^{II}_2(imH)_2(H_2O)_4[Nb^{IV}(CN)_8]\cdot 4H_2O\}_n \leftrightarrow \{Mn^{II}_2(imH)_2[Nb^{IV}(CN)_8]\}_n$ reported by us[18] are reversible. In this case, however, small water molecules can easily reenter the structure of the system after dehydration and the reverse process is possible.

3.2. Magnetic Studies. *Magnetic Properties of* α. Formula unit of $\{[Mn^{II}(urea)_2(H_2O)]_2[Nb^{IV}(CN)_8]\}_n$ α

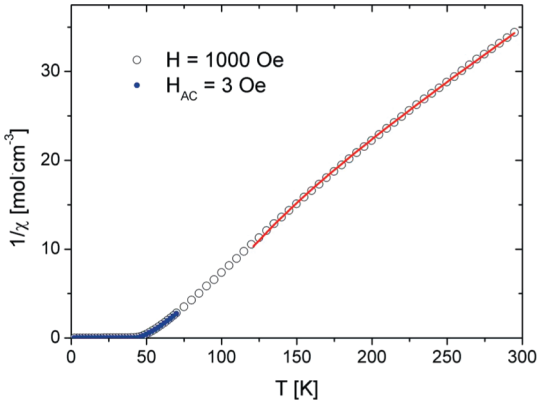

Figure 5. Inverse dc susceptibility of α measured on powder sample at H = 1kOe and ac susceptibility measured at H_{ac} = 3 Oe. The solid line was calculated using the mean-field model for a simple ferrimagnet (see text).

comprise two high-spin Mn^{II} (S = 5/2) and one Nb^{IV} (S = 1/2) with expected isotropic g-factors equal to 2.00.[16−18] Because of the 6:3 connectivity type, each Nb^{IV} magnetic moment interacts with six Mn^{II} ions and each magnetic moment of Mn^{II} interacts with three Nb^{IV} ions through −CN- bridges, creating a 3D magnetic lattice. Inverse susceptibility of the powder sample of α (Figure 5) deviates from the Curie−Weiss law, even after careful correction for diamagnetic contributions.[34a] The solid line in Figure 5 is the result of fitting experimental data above 120 K using the mean-field model for two sublattices, neglecting interactions other than Mn−Nb exchange[34b]

$$\chi = \frac{(2C_{5/2} + C_{1/2})T + 4\lambda C_{5/2}C_{1/2}}{T^2 - 2\lambda^2 C_{5/2}C_{1/2}}$$

where $C_S = N_A g^2 S(S+1)\beta^2/3k_B$ denotes the Curie constants for respective spins and $\lambda = 6J_{Mn-Nb}/(N_A g^2 \beta^2)$ is the molecular field constant and other symbols have their usual meaning (with the isotropic interaction Hamiltonian defined as follows: $\boldsymbol{H} = -J_{Mn-Nb}S_{Mn}S_{Nb}$). The values of g = 1.98(2) and λ = −44.5(2) mol/cm^3 were obtained from the fit, meaning that the predominant Mn−Nb interaction in α is antiferromagnetic.

Magnetic properties of α presented below were obtained for top-cut pyramidal-shaped single crystal sample (Figure 6). The mass of the used single crystal (m = 1.31 mg) was checked using $M(H)$ measured with much larger powder sample. At T_c = 43 K the measured magnetic moment rapidly increases (see Figure 7 for $M(T)$ at 1000, 250, and 100 Oe and Figures SI-6 and SI-7 in the Supporting Information for ac susceptibility and low field ZFC/FC data) indicating that **α** undergoes the transition to an ordered state with a large ferrimagnetic component. The $M(H)$ dependence for the single crystal measured at T = 2 and 30 K with the magnetic field applied along a and c crystallographic axes is shown in Figure 8. The magnetization very quickly saturates at 9.0(1) Nβ, which strongly suggests a collinear, ferrimagnetic ordering with two Mn 5β magnetic moments opposite to 1β of Nb. The perfectly constant $M(H)$ up to 50 kOe (not shown) at 2 K agrees with the fact that the Nb spin-flip transition, simulated in the mean field model, takes place above 1200 kOe. The c crystallographic direction is the magnetic hard axis and a (≡b) is the easy axis; the anisotropy field is small and equals 1.1 kOe. The temperature dependence of the magnetization measured along the easy axis a is presented in Figure 7. At the applied field 1 kOe, the whole sample is a single magnetic domain, and the magnetization 9$N\beta$ is reached at low T. At smaller fields, e.g. 100 Oe, the $M(T)$ is cut by the demagnetization field and multidomain effects. All magnetic measurements point out that α is a soft 3D ferrimagnet. The lack of the magnetic hysteresis, negligible χ'', and only small difference between ZFC and FC magnetization curves correspond with small anisotropy constant. Such behavior is expected due to the lack of orbital moment for both Mn^{II} and Nb^{IV} ions.

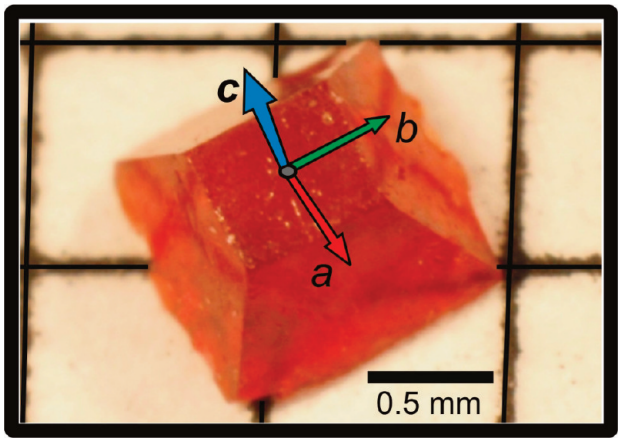

Figure 6. Photography of the top-cut pyramidal-shaped single crystal sample of α used for magnetic measurements with the scheme showing the orientation of the crystallographic axes.

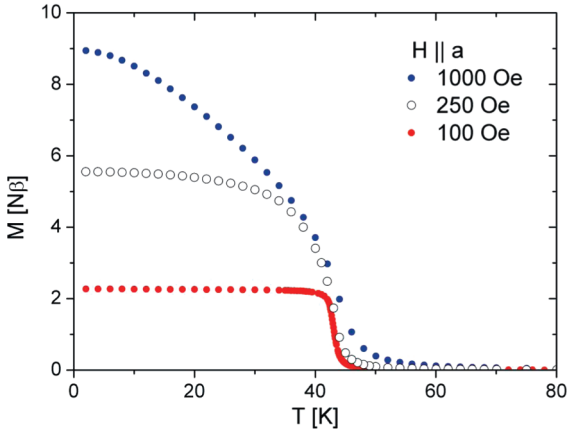

Figure 7. Magnetization vs temperature measured for magnetic field applied along the easy a axis of α. At 1 kOe applied field the moment saturates in low temperature and the data represent magnetization of a single domain sample. At smaller fields, demagnetization and multidomain effects cut the measured moment (blue points, 1 kOe; circles, 250 Oe; red points, 100 Oe).

Magnetic Properties of ***β***, ***2***, *and* ***3***. Results of magnetic measurements for polymorph β and the products of the transformation α/β → **2b** → **3** are very similar to those of α. The detailed description together with figures depicting $\chi(T)$ and $M(H)$ dependences of β, **2b**, and **3** can be found in the Supporting Information section. The ordering

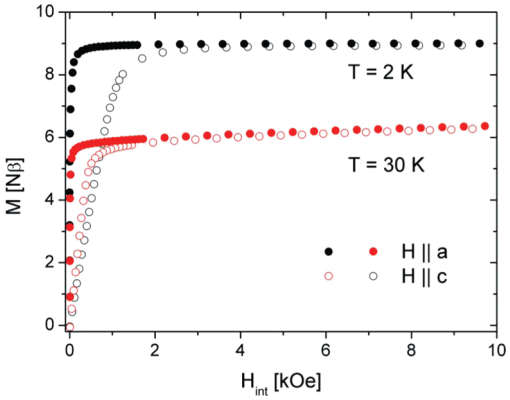

Figure 8. Magnetization vs magnetic field measured at $T = 2$ (in black) and 30 K (in red) along *a* (full points) and *c* (circles) axes of single crystal of α. Data were corrected for demagnetization field. At 2 K from 4 to 50 kOe no measurable change is observed.

temperatures T_c were estimated from ZFC/FC and AC magnetic measurements (see Figures SI-8, SI-9, and SI-10 in the Supporting Information) and are equal to 42, 70, and 47 K for *β*, **2b**, and **3**, respectively. The similar values of magnetization of saturation M_s (at 2 K), the results of the Curie−Weiss fit (C and θ_{CW} values) and mean-field model fit (g, λ, and J_{Mn-Nb}) presented in Table 2. all point out that *β*, **2b**, and **3** are magnets similar to α with possibly collinear ferrimagnetic ordering (two Mn magnetic moments opposite to that of Nb). The values of coupling constants J_{Mn-Nb} obtained for compounds α, *β*, and **3** where Mn^{II} centers are in nearly octahedral environment (−10.9, −10.3, and −10.4 cm^{-1}, respectively) are in good agreement with those reported previously for similar $Mn^{II}-Nb^{IV}$ cyanido-bridged systems: −6.8 cm^{-1} for $\{[Mn^{II}(pyrazole)_4]_2[Nb^{IV}(CN)_8]\cdot 4H_2O\}_n$,[37] and −13.6 cm^{-1} for nonanuclear Mn_6Nb_3 clusters.[38]

The values of magnetic ordering temperatures T_c of the $\{[Mn^{II}(urea)_2(H_2O)]_2[Nb^{IV}(CN)_8]\}_n$ molecular system varies from 43/42 K through 70 and back to 47 K depending on the structural transformations α/*β*→**2b**→**3** (Figure 9) but its soft ferrimagnetic character remains intact. Significant increase of the T_c at the first stage of transformation α/*β* → **2b** corresponds well with the proposed increase of the connectivity type. Another reason for the increased critical temperature and the increased value of the $J_{Mn-Nb} = -15.1$ cm^{-1} in **2b** might be the possible reduction of the coordination number of Mn^{II} from 6 to 5 after removal of urea ligands. Dependence of the strength of magnetic interactions on the connectivity of the network and the coordination number is well-documented in the literature (connectivity type;[16−18] coordination number[18,39]). At the second stage **2b** → **3**, the T_c decreases from 70 to 47 K due to the hydration process. The possibly empty sites in the coordination sphere of Mn^{II} are taken up by water molecules and its coordination number increase back to 6.

It was not possible to investigate the magnetic properties of pure **2a** because of its instability and significant loss of MeOH (ZFC-FC curves measured in liquid methanol shows at least two ferromagnetic transitions around 54 and 68 K suggesting partial transformation into **2b**, Figure SI-11 in the Supporting Information).

3.3. MSHG Effect. The thermal variation in the SH intensity has been measured for α single crystal (Figure 6). Between 100 and 50 K, the SH intensity stays constant within the experimental error. It then increases by 4.1 times when the temperature is further decreased down to 10 K (Figure 10). The temperature dependence of the SH intensity follows the thermal evolution of the magnetization of the compound (Figure 7).

The observed MSHG/SHG signal ratio was the largest among molecule-based noncentrosymmetric magnets.[8,40] The SHG and MSHG observed in α is understood by the following. It is known that the tensor element of the SH susceptibility (χ_{ijk}) is related to SH polarization (P_i) as follows: $P_i = \chi_{ijk}E_jE_k$, where i, j, and k are the coordinates, and E_j and E_k are the electric field of the incident wave. The crystal is tetragonal with a noncentrosymmetric space group ($P4_1$), and hence, SHG is permitted. This space group has the following nonzero elements in crystallographic term (χ^c_{ijk}): χ^c_{zzx}, χ^c_{zyy}, χ^c_{zzz}, χ^c_{xyz}, χ^c_{yyz}, χ^c_{xzx}, and χ^c_{yzx}. Furthermore, below T_c, the magnetic ordering creates a magnetic term (χ^m_{ijk}). Since the direction of the electric polarization (*c*-axis) and that of magnetic direction (*a* or *b*-axis) is orthogonal in the ferrimagnetic phase of α, magnetic point group is $P2_1$. In this situation, the SH susceptibility is described by the following equation.

$$\begin{pmatrix} P_x \\ P_y \\ P_z \end{pmatrix} = \begin{pmatrix} \chi^m_{xxx} & \chi^m_{xyy} & \chi^m_{xzz} & \chi^c_{xyz} & \chi^c_{xzx} & \chi^m_{xxy} \\ \chi^m_{yxx} & \chi^m_{yyy} & \chi^m_{yzz} & \chi^c_{yyz} & \chi^c_{yzx} & \chi^m_{yxy} \\ \chi^c_{zxx} & \chi^c_{zyy} & \chi^c_{zzz} & \chi^m_{zyz} & \chi^m_{zzx} & 0 \end{pmatrix} \begin{pmatrix} E_xE_x \\ E_yE_y \\ E_zE_z \\ 2E_yE_z \\ 2E_zE_x \\ 2E_xE_y \end{pmatrix} \quad (1)$$

Upon the irradiation with p-polarized incident light, nonlinear polarization is given by

$$\begin{pmatrix} P_x \\ P_y \\ P_z \end{pmatrix} = \begin{pmatrix} \chi^m_{xxx} \\ \chi^m_{yxx} \\ \chi^c_{zxx} \end{pmatrix} E_xE_x + \begin{pmatrix} \chi^m_{xzz} \\ \chi^m_{yzz} \\ \chi^c_{zzz} \end{pmatrix} E_zE_z + 2\begin{pmatrix} \chi^c_{xzx} \\ \chi^c_{yzx} \\ \chi^m_{zzx} \end{pmatrix} E_zE_x \quad (2)$$

(37) Pinkowicz, D.; Pełka, R.; Drath, O.; Nitek, W.; Bałanda, M.; Majcher, A. M.; Poneti, G.; Sieklucka, B. *Inorg. Chem.* **2010**, *49*, 7565–7576.
(38) Venkatakrishnan, T. S.; Rajamani, R.; Ramasesha, S.; Sutter, J.-P. *Inorg. Chem.* **2007**, *46*, 9569–9574.
(39) (a) Larionova, J.; Sanchiz, J.; Golhen, St.; Ouahab, L.; Kahn, O. *Chem. Commun.* **1998**, 953. (b) Tanase, St.; Tuna, F.; Guionneau, Ph.; Maris, Th.; Rombaut, G.; Mathonière, C.; Andruh, M.; Kahn, O.; Sutter, J.-P. *Inorg. Chem.* **2003**, *42*, 1625. (c) Milon, J.; Daniel, M.-Ch.; Kaiba, A.; Guionneau, Ph.; Brandes, St.; Sutter, J.-P. *J. Am. Chem. Soc.* **2007**, *129*, 13872.
(40) (c) Nuida, T.; Matsuda, T.; Tokoro, H.; Sakurai, S.; Hashimoto, K.; Ohkoshi, S. *J. Am. Chem. Soc.* **2005**, *127*, 11604. (d) Ikeda, K.; Ohkoshi, S.; Hashimoto, K. *J. Appl. Phys.* **2003**, *93*, 1371.

Table 2. Selected Results of Magnetic Measurements for α, *β*, 2b, and 3

			Curie−Weiss fit (above 150 K)		mean-field model fit (above 120 or 150 K*)		
	T_c (K)	M_s (Nβ)	C (cm^3 mol^{-1} K)	θ_{CW} (K)	g	λ (mol cm^{-3})	J_{Mn-Nb} (cm^{-1})
α	43	9.0(1)	7.5(1)	33.0(5)	1.98(2)	−44.5(2)	−10.9(5)
β	42	8.9(1)	7.5(1)	31.0(5)	1.96(3)*	−43.0(3)*	−10.3(7)
2b	70	9.3(1)	7.1(1)	61.0(5)	2.01(3)	−59.8(5)	−15.1(8)
3	47	8.6(1)	7.1(1)	34.0(5)	1.93(4)	−44.8(3)	−10.4(8)

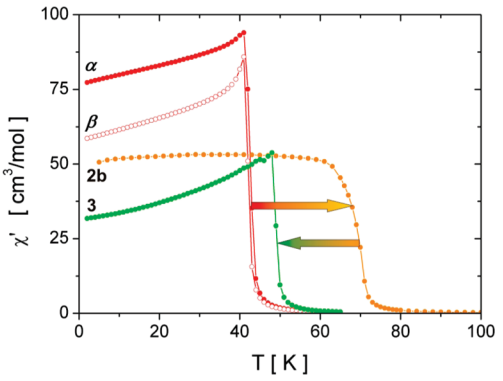

Figure 9. Changes of the T_c values in the α/*β* → **2b** → **3** transformation sequence (ac magnetic susceptibilities at H_{ac} = 3 Oe and f = 10 Hz; red pionts, α; red circles, *β*, orange points, **2b**; green points, **3**; solid lines are guides for the eye).

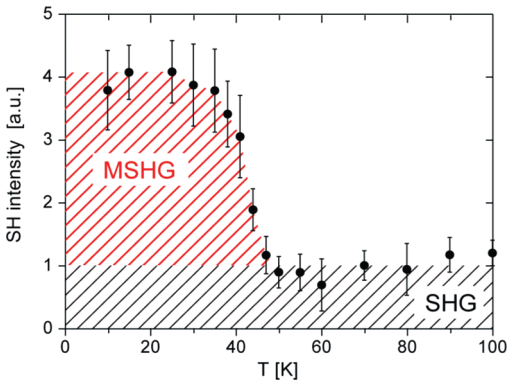

Figure 10. Thermal variation in the SHG signal for a single crystal of α in a 500 G magnetic field applied along the *a*-axis.

The χ^m_{ijk} terms operate below T_c, and hence, SH intensity is enhanced. Because χ^m_{ijk} is related to the magnitude of local magnetization, it increases near T_c due to the spontaneous magnetization.

The MSHG at 532 nm is caused by the d−d electronic transition from $d_{x^2-y^2}$ to d_{z^2} on $[Nb(CN)_8]^{4-}$ dodecahedron, which is obtained by DV-Xα molecular orbital calculation (see Figure SI-12 in the Supporting Information). The magnetic orbital of $d_{x^2-y^2}$ on Nb^{IV} (S = 1/2) directly couple with d−d transition, and hence the large enhancement of MSHG was observed through the spin−orbital coupling on Nb^{IV} (ζ = c.a. 850 cm^{-1}).

4. Conclusions

Following the molecular approach to the construction of multifunctional magnetic molecular materials (4Ms), we have successfully introduced urea molecules into the 3D magnetic network based on Mn^{II} and $[Nb^{IV}(CN)_8]^{4-}$. As a result, we have obtained two polymorphs of $\{[Mn^{II}(urea)_2(H_2O)]_2[Nb^{IV}(CN)_8]\}_n$ system: chiral α and centric *β*. Both polymorphs are classical soft ferrimagnets, which show identical topology, connectivity and have extremely similar structures but crystallize in different space groups $P4_1$ and $P\bar{1}$, respectively. In polymorph *β* the possible NLO functionality is quenched by its centro-symmetry, while in case of α the pyroelectric space group $P4_1$ allows its occurrence as SHG phenomena. Additionally below magnetic ordering temperature of 43 K polymorph α shows magnetization-induced SHG due to the interaction of both NLO and magnetic functionalities.

Both $\{[Mn^{II}(urea)_2(H_2O)]_2[Nb^{IV}(CN)_8]\}_n$ polymorphs exhibit also similar and complex reactivity based on the incorporated urea molecules. Both compounds adapt their structures to the changing chemical environment, forming amorphous $\{[Mn^{II}(H_2O)]_2[Nb^{IV}(CN)_8]\cdot 2.5MeOH\}_n$ **2b** with increased connectivity and reduced coordination number of Mn^{II} centers in methanol and subsequently well-known crystalline compound $\{[Mn^{II}(H_2O)_2]_2[Nb^{IV}(CN)_8]\cdot 4H_2O\}_n$ **3** in water vapors. The structural conversions are followed by the dramatical shifts of the T_c from 43/42 K for α/*β* to 70 K for **2b** and 47 for **3**.

The thermal variation in the SH intensity has been measured for α single crystal. Between 100 and 50 K, the SH intensity stays constant within the experimental error. It then increases by 4 times when the temperature is further decreased down to 10 K. The temperature dependence of the SH intensity follows the thermal evolution of the magnetization of the compound. Hence, this increase was attributed to MSHG and was understood by the generation of magnetic term of nonlinear susceptibility. To the best of our knowledge, the observed MSHG/SHG signal ratio was the largest among molecule-based noncentrosymmetric magnets. This observation is a significant result in both fields of magnetooptics and magnetic materials because reports of bulk MSHG phenomenon are very limited.

Acknowledgment. This work was financed by the Polish Ministry of Science and Higher Education within Research Project 0538/B/H03/2008/35 and partially within Research Project 1535/B/H03/2009/36. The present research was also supported in part by a Grant-in-Aid for Young Scientists (S) from JSPS, a Grant for the Global COE Program "Chemistry Innovation through Cooperation of Science and Engineering", the Photon Frontier Network Program, and a Grant-in-Aid for Young Scientists (B) from MEXT (Japan). Elemental Analyses were carried out using equipment purchased thanks to the financial support of the European Regional Development Fund in the framework of the

Polish Innovation Economy Operational Program (Contract POIG.02.01.00-12-023/08).

Supporting Information Available: Structure models of α and *β* in CIF format and the table with selected crystallographic data; detailed results of the CShM Analysis for the coordination spheres of Mn1, Mn2 and Nb in α and *β*; additional structural diagrams of α and *β*; IR spectra of α, *β*, **2a**, **2b**, **3**, urea and $K_4[Nb(CN)_8]$ with the extended description; magnetic data and figures of *β*, **2a**, **2b**, and **3** with the extended description; energy diagram and orbitals of $[Nb(CN)_8]^{4-}$ in polymorph α. This material is available free of charge via the Internet at http://pubs.acs.org.